

# Resonant Regimes in the Fock-Space Coherence of Multilevel Quantum dots

Eduardo Vaz and Jordan Kyriakidis\*

(Dated: July 11, 2021)

## Abstract

The coherence between quantum states with different particle numbers — the Fock-space coherence — qualitatively differs from the more common Hilbert-space coherence between states with equal particle numbers. For a quantum dot with multiple channels available for transport, we find the conditions for decoupling the dynamics of the Fock-space coherence from both the Hilbert-space coherence as well as the population dynamics. We further find specific energy and coupling regimes where a long-lived resonance in the Fock-space coherence of the system is realized, even where no resonances are found either in the populations or Hilbert-space coherence. Numerical calculations show this resonance remains robust in the presence of both boson-mediated relaxation and transport through the quantum dot.

PACS numbers: 72.10.Bg, 73.21.La, 73.23.-b, 73.23.Hk

## I. INTRODUCTION

According to quantum theory, a physical system can exist in a coherent superposition of distinct values of a single physical observable. One such superposition is over the number of particles present in the system. Such Fock-space coherence (FSC) has been recently and controllably demonstrated in bosonic systems.<sup>1-3</sup> The lifetime of these novel states may be considerably enhanced due to the near quenching of single-particle relaxation channels. This mitigation of both decay and decoherence is a prime requisite, for example, in the demonstration of scalable quantum information processing architectures. In Fermionic systems such as charge carriers in a quantum dot, the influence of Fock states on the dynamics and transport properties has been investigated<sup>4-6</sup> but not the coherence properties of the states themselves. Here we show that coherent fermionic Fock states in multilevel quantum dots can exhibit decoherence times at least an order of magnitude greater<sup>7</sup> than the more conventional Hilbert-space coherence (HSC) between states with fixed particle number. This estimate remains valid even in the presence of a strong perturbation such as resonant tunnelling transport through the system as well as coupling to a bosonic bath. Our fully non-Markovian calculations reveal a memory-kernel whose elements factorise into non-interacting blocks, one of which contains all of the Fock-coherence. Our results are independent of the number of tunnelling pathways available through the system, although more than one seems necessary, indicating that an interference effect may be responsible for the robustness of these states. Our results further demonstrate how novel quantum states can exhibit remarkably useful properties given careful—though not prohibitive—tuning of bias, level spacing, and barrier anisotropy of the system.

## II. MODEL

Our model is that of a single quantum dot weakly coupled to biased source and drain semi-infinite leads, such that only a small number of electronic channels are available for transport. We also consider particle-preserving relaxation through a coupling to a bosonic reservoir (phonons, for example). The total Hamiltonian is given by

$$H = H_{\text{leads}} + H_{\text{qd}} + H_{\text{boson}} + \mathcal{H}_{\mathcal{T}} + \mathcal{H}_{\mathcal{R}}, \quad (1)$$

where  $H_{\text{leads}} = \sum_{s(d)} (\epsilon_{s(d)} \pm \frac{1}{2} eV_b) d_{s(d)}^\dagger d_{s(d)}$  describes the source and drain leads as non-interacting fermion systems shifted by the bias voltage  $V_b$ . The creation and annihilation operators for the source (drain) leads are  $d_{s(d)}^\dagger, d_{s(d)}$ , respectively, and  $\epsilon_{s(d)}$  are the respective single-particle energies. The quantum dot in the non-interacting regime is given by  $H_{\text{qd}} = \sum_i (\hbar\omega_i + eV_g) c_i^\dagger c_i$ , where  $c_i^\dagger$  and  $c_i$  are system creation and annihilation operators, and the single-particle energies  $\hbar\omega_i$  are all shifted by the applied gate voltage,  $V_g$ . For the sake of clarity we neglected Coulomb interactions throughout the paper, as these are not expected to qualitatively change the results beyond an energy-level renormalization.<sup>8,9</sup> The coupling to the electronic reservoirs is described by a tunnelling Hamiltonian,  $\mathcal{H}_{\mathcal{T}} = \sum_{i,r=(s,d)} (T_i^r d_r^\dagger c_i + \text{h.c.})$ , where  $T_i^{s(d)}$  is an energy-independent tunnelling coefficient for a particle tunnelling from the single-particle state  $|i\rangle$  in the dot to the source (drain) reservoir<sup>10</sup>. We consider the qualitative effects of a boson-mediated relaxation on the FSC, and introduce a bosonic reservoir and its interaction with the quantum dot, described respectively by  $H_{\text{boson}} = \sum_l \epsilon_l b_l^\dagger b_l$ , and  $\mathcal{H}_{\mathcal{R}} = \sum_{i,j,l} (A_{ijl} c_i^\dagger c_j b_l + \text{h.c.})$ , where  $A_{ijl}$  is a generic coupling coefficient containing the details of a specific electron-boson interaction.

### III. TIME EVOLUTION AND THE MEMORY KERNEL

The non-Markovian time evolution of the quantum dot is considered in the weak coupling approximation (Born approximation), where terms up to second order in the interaction Hamiltonians  $\mathcal{H}_{\mathcal{T}}$  and  $\mathcal{H}_{\mathcal{R}}$  are kept.

The generalized master equation for the reduced density matrix<sup>11</sup> is given by

$$\dot{\rho}_{ab}(t) = \sum_{c,d} \int_0^t dt' \rho_{cd}(t') \Upsilon_{abcd}(t-t') e^{i\gamma_{abcd}t'}, \quad (2)$$

where the total memory kernel  $\Upsilon_{abcd}(t)$  describing the dynamics of the system can be explicitly derived<sup>12</sup> directly from the microscopic Hamiltonian Eq. (1). Under a weak coupling approximation  $\Upsilon_{abcd}(t)$  can be written as the sum of a transport-dependent ( $\mathcal{T}$ ) and relaxation-dependent ( $\mathcal{R}$ ) transition tensors,

$$\Upsilon_{abcd}(t) = \mathcal{T}_{abcd}(t) + \mathcal{R}_{abcd}(t). \quad (3)$$

The absence of bilinear terms in the interaction Hamiltonians  $\mathcal{H}_{\mathcal{T}}$  and  $\mathcal{H}_{\mathcal{R}}$  is due to the trace over the electronic reservoirs, where terms of the form  $\langle r|d_l|r\rangle = \langle r|d_l^\dagger|r\rangle = 0$ .

The transition tensor  $\mathcal{T}$  due to electronic transport is given by,

$$\begin{aligned} \mathcal{T}_{abcd}(t) = \sum_{\alpha,\beta,r} \left\{ K_{\alpha\beta}^r \left[ \Omega_{\phi_B,\mu^r}^\alpha(t) \Delta_{badc}^{\alpha\beta} - \Omega_{\phi_T,\mu^r}^\alpha(t) \Delta_{cdab}^{\alpha\beta} \right] \right. \\ \left. + K_{\beta\alpha}^r \left[ \Omega_{\phi_B,\mu^r}^{\alpha*}(t) \Delta_{abcd}^{\alpha\beta} - \Omega_{\phi_T,\mu^r}^{\alpha*}(t) \Delta_{dcba}^{\alpha\beta} \right] \right\}, \end{aligned} \quad (4a)$$

with,

$$\Omega_{x,y}^\alpha(t) = (e^{i\omega_{x\alpha}t} - e^{i\omega_{y\alpha}t}) / t, \quad (4b)$$

$$K_{\alpha\beta}^r \equiv iN_r (T_\alpha^r)^* T_\beta^r / \hbar, \quad (4c)$$

$$\Delta_{abcd}^{\alpha\beta} \equiv \langle a|c_\alpha^\dagger|c\rangle \langle d|c_\beta|b\rangle - \langle a|c\rangle \langle b|c_\alpha c_\beta^\dagger|d\rangle, \quad (4d)$$

and where the Latin indexes denote many-body system states, Greek indexes denote single-particle states, and  $r = s$ ,  $d$  denotes the source and drain leads. Both leads are assumed to be metallic with occupied-state energies lying between a lower bound  $\phi_B$  and the lead's chemical potential  $\mu^{s(d)}$ , and unoccupied-state energies lying between the lead's chemical potential and an upper bound  $\phi_T$ . The range between the bounds  $\phi_B$  and  $\phi_T$  are taken to be large relative to the characteristic energies of the system. Finally,  $N_r$  denotes the density of states in lead  $r$ , and the frequencies  $\omega_{ij} \equiv \omega_i - \omega_j$ .

Similarly, the transition tensor due to boson-mediated relaxation is given by

$$\begin{aligned} \mathcal{R}_{abcd}(t) = G \sum_{ijpqk} \left[ M_{ijpqk} (\Theta_{ijpq}^{abcd} e^{i\omega_{ijk}t} + \Theta_{pqij}^{abcd} e^{-i\omega_{ijk}t}) \right. \\ \left. + M_{ijpqk}^* (\Theta_{ijpq}^{dcba} e^{i\omega_{ijk}t} + \Theta_{pqij}^{dcba} e^{-i\omega_{ijk}t}) \right] \end{aligned} \quad (5a)$$

where,

$$\Theta_{ijpq}^{abcd} = \langle a|c_i^\dagger c_j|c\rangle \langle d|c_q c_p^\dagger|b\rangle - \langle b|d\rangle \langle a|c_q^\dagger c_p c_j c_i^\dagger|c\rangle, \quad (5b)$$

$$M_{ijpqk} = A_{ijk} A_{pqk}^*, \quad (5c)$$

and  $G$  is the density of states of the boson reservoir.

#### IV. TWO TRANSPORT CHANNELS

The transport and relaxation transition tensors presented in Eqs. (4, 5), are for a general number of available transport channels. For  $k$  transport channels, a minimum of  $2^k$  dy-

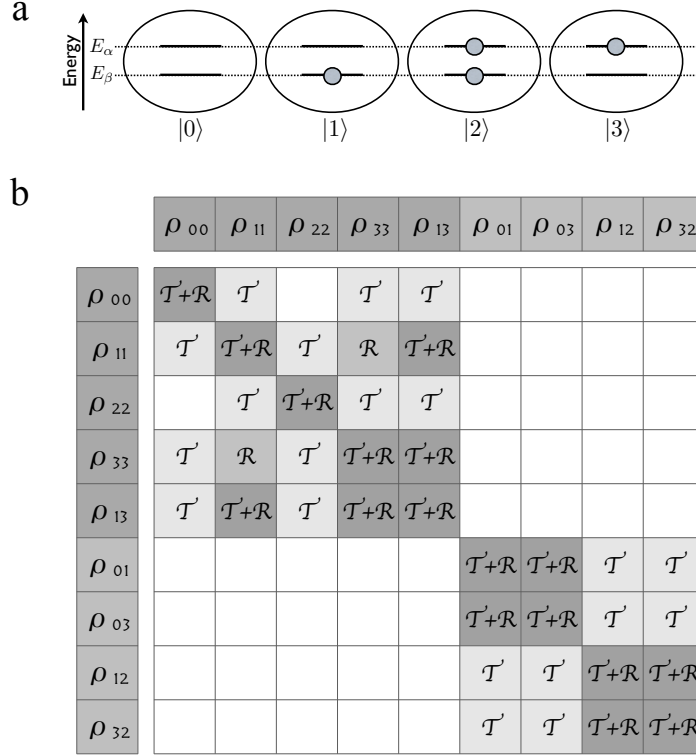


FIG. 1. (a) Basis states for the two-channel case, defined as  $|0\rangle = |N - 1\rangle_{\text{gs}}$ ,  $|1\rangle = |N\rangle_{\text{gs}}$ ,  $|2\rangle = |N + 1\rangle_{\text{gs}}$ , and  $|3\rangle = |N\rangle_{\text{es}}$ . (b) Representation of the non-zero memory kernel elements for the case of two transport channels. In the figure, the matrix elements represent the contributions to the dynamics between the reduced density matrix elements shown in the outermost row and column, due to transport ( $\mathcal{T}$ ), bosonic relaxation ( $\mathcal{R}$ ), or both. Not all elements of  $\Upsilon_{abcd}$  are depicted; missing elements are the complex conjugates of those present.

namical states are required, yielding  $2^{2k}$  density matrix elements and  $2^{4k}$  transition tensor components determining the dynamics of the system; despite symmetry-induced reductions in the number of independent components, the computational cost nevertheless increases exponentially with the number of channels. In what follows, we focus on the simplest non-trivial case of two available transport channels.

The two-channel model is schematically depicted in Fig. 1a. States  $|0\rangle$ ,  $|1\rangle$ , and  $|2\rangle$  respectively denote ground states with  $N - 1$ ,  $N$ , and  $N + 1$  confined particles and state  $|3\rangle$  denotes an  $N$ -particle excited state. This is an experimentally accessible regime.<sup>13</sup> The non-vanishing components of the memory kernel are shown in Fig. 1b. The cell in the row labelled  $\rho_{ab}$  and column  $\rho_{cd}$  indicates whether the element  $\Upsilon_{abcd}$  is zero (empty cell) or depends

on a combination of transport ( $\mathcal{T}$ ) or boson-mediated relaxation ( $\mathcal{R}$ ). For example, only transport contributes to  $\Upsilon_{3300}$ , only bosonic relaxation contributes to  $\Upsilon_{1133}$ , both transport and bosonic relaxation contribute to  $\Upsilon_{1113}$ , and  $\Upsilon_{0022}$  vanishes. Elements not depicted in the figure may be inferred through the relation  $\Upsilon_{abcd} = \Upsilon_{badc}^*$  for  $a \neq b$  and  $c \neq d$ .<sup>14</sup> As expected, the only transitions where relaxation alone ( $\mathcal{R}$ ) carries the dynamics are between states with the same number of particles ( $|1\rangle$  and  $|3\rangle$  in this case).

In this matrix representation of the tensor  $\Upsilon_{abcd}$ , two decoupled sub-matrices are apparent. The upper sub-matrix represents dynamics among population probabilities and coherence in states with identical particle number (HSC). The lower block describes coherence between states differing by one particle. Thus, the lower block describes the evolution of the FSC and is decoupled from the HSC.

The decoupling of the FSC dynamics is not a result of the number of channels involved. For example, increasing the bias to allow more transport channels will increase the number of relevant elements of  $\Upsilon_{abcd}$ . The structure that emerges is similar to that depicted in Fig. 1b, but the blocks themselves increase in both size and number; the FSC blocks remain decoupled from the HSC. Fundamentally, the structure is due to the fact that fermions cannot be individually created or destroyed through a scattering event (as opposed to bosonic systems). Since a bosonic bath does not alter the structure of the transition tensor, and since the time scale set by resonant tunnelling is generally much faster than that set by the bosonic coupling, we shall restrict ourselves to the transport problem and neglect the bosons in the remainder.

A solution to the evolution equations, Eq. (2), is obtained<sup>11</sup> by moving to Laplace space and using the convolution theorem to transform the integrodifferential equations to a coupled set of algebraic equations. We numerically uncouple these equations and then transform back to the time domain by means of a Bromwich integral<sup>15</sup>.

The present transport model is described by seven parameters: Fermi energy  $E_F$ , bias voltage  $V_b$ , gate voltage  $V_g$ , energy-level spacing  $\Delta E = E_\alpha - E_\beta$ , orbital anisotropy  $\varepsilon = 1 - T_\beta^s/T_\alpha^s = 1 - T_\beta^d/T_\alpha^d$ ,<sup>16</sup> barrier asymmetry  $\lambda = T_\alpha^d/T_\alpha^s = T_\beta^d/T_\beta^s$ , and overall tunnel-coupling strength set by  $T_\alpha^s$ . The orbital anisotropy  $\varepsilon$  describes differences in the tunnel coupling strength to different orbitals in the system. We define *edge* and *core* orbitals by the relative strength of their coupling to the reservoirs owing to the detailed shape of the wave function and the relative penetration into the tunnelling barriers.<sup>17</sup> In relation to the

Parameter	$E_F$	$eV_B$	$eV_g$	$\Delta E$	$\varepsilon$	$\lambda$	$T_\alpha^s$
Value	30 meV	6 meV	0 meV	2 meV	1	1	0.5 meV

TABLE I. Standard set of parameter values used throughout the present work. Unless otherwise noted, these values were used for all results presented.

2-channel case illustrated in Fig. 1a, we denote orbitals  $|\alpha\rangle$  and  $|\beta\rangle$  as the edge and core orbitals respectively.

In what follows, we plot our results as a function of one or two parameters while fixing the others to a set of “standard values.” The standard values of the parameters are given in Table I, which exhaustively describes our energetic configuration. For example, the two orbital levels have an energy of  $E_{\alpha,\beta} = E_F \pm \frac{\Delta E}{2} + eV_g$ .

## V. FSC RESONANCE

We focus on the density-matrix element  $\rho_{01}(t)$  which describes the FSC between the  $N-1$  and the  $N$ -particle ground states. (See Fig. 1a.) The initial conditions for the density-matrix have an effect only on the amplitude of oscillations of the FSC, and not on the presence or location of a resonance. Thus, for the results presented here we choose a homogeneous initial FSC distribution as  $\rho_{01}(0) = \rho_{03}(0) = \rho_{12}(0) = \rho_{32}(0) = 0.1$ .

The time evolution of the FSC element  $\rho_{01}(t)$  is shown in Fig. 2a as a function of orbital anisotropy  $\varepsilon$  (horizontal axis), where  $T_\beta = \chi T_\alpha$  with  $0 \leq \chi \leq 1$ . For all but a narrow range around  $\varepsilon_{\text{res}} \approx 0.22$ , the coherence drops off rapidly, within approximately 3 ps, corresponding to only a few tunnelling events ( $\hbar/T_\alpha \approx 0.7$  ps). This mirrors the decay found in the HSC,<sup>11</sup> described, for example, by the matrix element  $\rho_{13}(t)$ . Remarkably, at an orbital anisotropy of  $\varepsilon_{\text{res}} \approx 0.22$ , we observe a resonance in the FSC. The coherent oscillations persist for a far greater length of time. This resonance is unique to the FSC elements of  $\rho(t)$ ; they do not occur in either the HSC or the population probabilities  $\rho_{nn}(t)$ . To our knowledge, this is the first demonstration of a resonance in the Fock-Space coherence of an open quantum system of fermions.

Figure 2b shows the Fourier spectrum of the time-domain results shown in Fig. 2a. At a given  $\varepsilon$ , two frequencies dominate the spectrum. One is a high-frequency component which

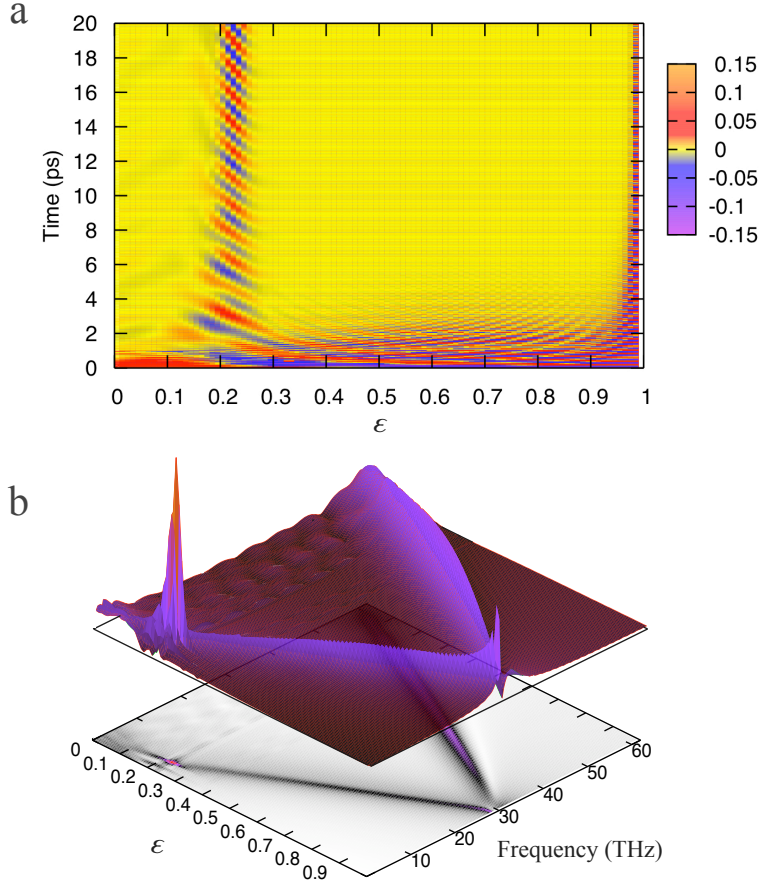


FIG. 2. (a) Time evolution of the FSC element  $\rho_{01}(t)$  as a function of the orbital anisotropy  $\varepsilon$ . A resonance in the FSC is observed at an anisotropy of  $\varepsilon_{\text{res}} \approx 0.22$  that maintains a persistent coherence well beyond the expected decoherence time. (b) Fourier transform of the results in (a). A linear dependence between frequency and  $\varepsilon$  is evident. A spike in the low frequency amplitude occurs at the resonant anisotropy of  $\varepsilon = 0.22$ . From this peak, we obtain the resonant frequency as given by Eq. (7).

decreases linearly with  $\varepsilon$ . This is the frequency related to the fast decay of the HSC, the population probabilities, and the FSC at very short times. There is also a low-frequency component evident in Fig. 2b, corresponding to slow envelope oscillations. The resonance, clearly seen as the spike in Fig. 2b, occurs on this low-frequency line.

The resonant orbital anisotropy  $\varepsilon_{\text{res}}$  depends on the opacity of the source and drain barriers as well as on the overall strength of the tunnel couplings. Figure 3a shows  $\rho_{01}$  in the long-time limit (defined as the time beyond which the transients have decayed—

approximately 10 ps in the present case) as a function of both orbital anisotropy  $\varepsilon$  and barrier asymmetry  $\lambda$ . The evident peak (resonance) in the amplitude of  $\rho_{01}$  at this long-time limit gives the position of the resonant orbital anisotropy as a function of the barrier asymmetry. We observe a strong relationship between  $\lambda$  and  $\varepsilon_{\text{res}}$  whose form is obtained from an empirical analysis (discussed later in this paper), and shown superimposed on the calculated data on Fig 3a. A similar dependence is also obtained between the resonant orbital anisotropy and the overall tunnelling strength. In contrast, the dependence of  $\varepsilon_{\text{res}}$  on the energetics is rather weak. Figure 3b, for example, shows the FSC resonance, again in the long-time limit, as a function of orbital anisotropy  $\varepsilon$  and level spacing  $\Delta E \equiv E_\alpha - E_\beta$ , and exhibits a linear and much weaker dependence of  $\varepsilon_{\text{res}}$  on  $\Delta E$ . (Similar results are seen in the dependence of  $\varepsilon_{\text{res}}$  on the bias voltage  $V_b$ , and gate voltage  $V_g$ .)

As might be expected, the energetics of the system do play a role in the frequency of the coherent oscillations. Figure 4 plots the time evolution of the FSC element  $\rho_{01}(t)$  as a function of the orbital level spacing  $\Delta E$  for a resonant anisotropy  $\varepsilon_{\text{res}} = 0.22$ . The patterns seen in Figure 4 are suggestive of a coherent interference effect between tunnelling pathways as the source of the resonance. The strongest constructive interference for this set of parameters occurs for  $\Delta E \approx 1.5$  meV.

We have empirically deduced that the dominant frequencies  $\nu$  evident in Fig. 2b depend on the energy and coupling system parameters in the following way:

$$\nu_{\pm}(\varepsilon) = \left| E_F + eV_g - \frac{\Delta E}{2} \pm 2\ln(\phi_T)(T_\alpha^s)^2(1 + \lambda^2)(1 - \varepsilon) \right|. \quad (6)$$

We have further empirically deduced that the resonant frequency  $\nu_{\text{res}}$ , also evident in Fig. 2b, depends on the energetics of the system in the following way:

$$\nu_{\text{res}} = \frac{1}{2}(eV_b + \Delta E) + eV_g. \quad (7)$$

At resonance, Eqs. (6) and (7) describe the same frequency. Equating them yields the resonance anisotropy  $\varepsilon_{\text{res}}$  as a function of the Fermi energy, level-spacing, bias voltage, gate voltage, coupling strength, and barrier anisotropy:

$$\varepsilon_{\text{res}} = 1 - \left( \frac{E_F - \Delta E - \frac{1}{2}eV_b}{2\ln(\phi_T)(T_\alpha^s)^2(1 + \lambda^2)} \right). \quad (8)$$

The fits to the numerical results presented in Figs. 3a and 3b were produced according to Eq. (8). Note that there are no free fitting parameters in this result. These result

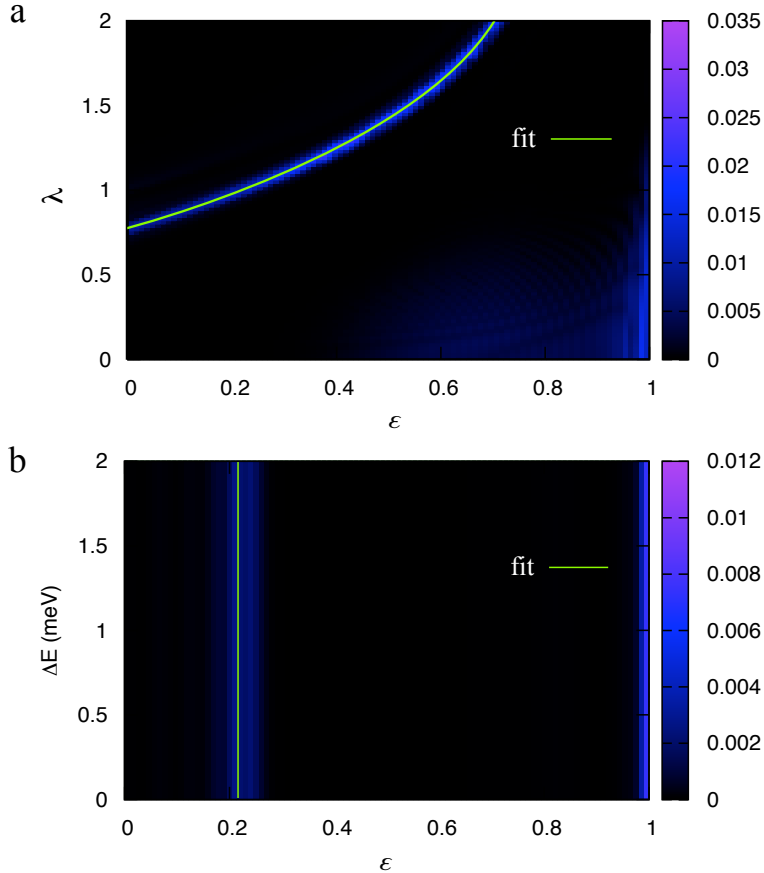


FIG. 3. (a) FSC element  $\rho_{01}$  in the long-time limit as a function of orbital anisotropy  $\varepsilon$ , and barrier asymmetry  $\lambda$ . The ridge denotes the resonance. (b) FSC element  $\rho_{01}$  at the long-time limit as a function of orbital anisotropy and energy level spacing. The fits displayed in both plots were produced according to Eq. (8).

may be used as an experimental guide when searching for this FSC resonance, as novel methods to extract electronic THz oscillations (equivalent to picosecond-range periods) are becoming accessible either by indirect electrooptical methods<sup>18,19</sup> or by means of high-Tc superconductor devices<sup>20</sup>.

## VI. SOURCE OF FSC RESONANCE

In order to address the source of the FSC resonance in our model, we consider the formation of a bound state between the quantum dot and the reservoirs.<sup>21–23</sup> Such a bound state may arise when the presence of a coupling term between the system and environment

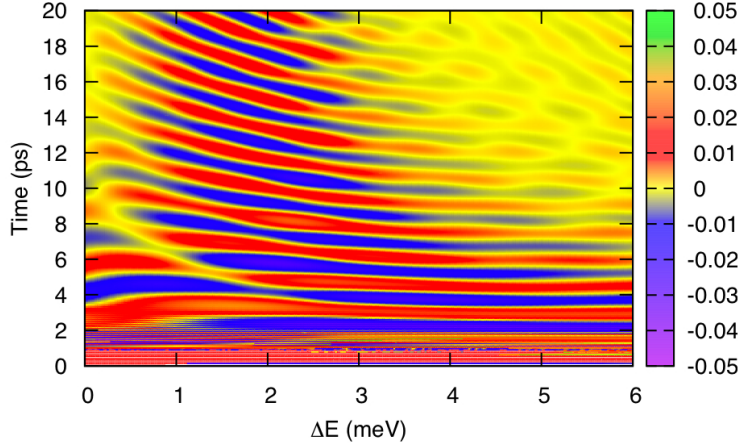


FIG. 4. Time evolution of the FSC element  $\rho_{01}(t)$  as a function of the level spacing within the bias window, and for a resonant orbital anisotropy  $\varepsilon = 0.22$ .

reduces the total energy.

Defining the bound state of the QD and the reservoirs as  $|\psi\rangle = |QD\rangle|R\rangle$ , where  $|QD\rangle = \sum_n P_n|n\rangle$  denotes the state of the QD, and  $|R\rangle = \sum_r \int_{\phi_B^r}^{\phi_T^r} f(\epsilon_k)|\epsilon_k\rangle d\epsilon_k$  denotes the continuum of reservoir states for  $r = \{s, d\}$ , we solve the eigenvalue equation  $H|\psi\rangle = E|\psi\rangle$  for the total energy of the  $E$ , with the total Hamiltonian  $H$  given by Eq. 1.

For a 2-channel case, the solution to the eigenvalue equation has the form,<sup>21</sup>,

$$\sum_{n'=0}^3 [E_n \delta_{n,n'} - \sum_{r=\{s,d\}} \int_{\phi_B^r}^{\phi_T^r} \frac{T_{n'}^r (T_n^r)^*}{\epsilon_k - E} d\epsilon_k] P_{n'} = E P_n. \quad (9)$$

We note that the integration limits over the reservoirs become truncated by the single creation and annihilation operators of the tunneling Hamiltonian to  $\int_{\phi_B^r}^{E_{Fermi}^r}$  for removing a particle from, and  $\int_{E_{Fermi}^r}^{\phi_T^r}$  for adding a particle to, reservoir  $r$ .

Therefore, the solution is found to be of the form,

$$Y(E) = E_0 - I_{\alpha,\alpha,E_3} - I_{\beta,\beta,E_1} - \frac{[I_{\alpha,\beta,E_1} + I_{\beta,\alpha,E_3}][I_{\alpha,\beta,E_3} + I_{\beta,\alpha,E_1}]}{E_2 - E - [I_{\alpha,\alpha,E_1} + I_{\beta,\beta,E_3}]} = E, \quad (10)$$

with,

$$I_{a,b,E_n} = E_n - E - \sum_{r=\{s,d\}} \left[ \int_{E_{Fermi}^r}^{\phi_T^r} \frac{T_a^r (T_b^r)^*}{\epsilon_k - E} d\epsilon_k + \int_{\phi_B^r}^{E_{Fermi}^r} \frac{T_a^r (T_b^r)^*}{\epsilon_k - E} d\epsilon_k \right]. \quad (11)$$

The existence of a bound state requires that  $Y(E)$  has at minimum one real solution for  $E < 0$ , which is equivalent to  $Y(0) < 0$  being satisfied. For the case of the transcendental

equation, Eq. 10, we find that the left hand side is monotonically decreasing with  $E$ , and the right hand side linearly increases with  $E$ , therefore there can be at most one solution where l.h.s. = r.h.s., and thus only one bound state. In the case of  $Y(0) < 0$ , we also see that under the approximation of energy-independent coupling coefficients, the integrals over  $\epsilon_k$  appearing in Eq. 11 lead to terms of the form  $\ln(\epsilon_k)|_{\epsilon_k=\{\phi_{(B,T)}^r, E_{Fermi}^r\}}$ . Using this, along with recalling the coupling anisotropies  $\lambda = T_n^d/T_n^s$  and  $\varepsilon = 1 - T_\alpha^r/T_\beta^r$  in order to define all coupling coefficients in terms of  $T_\alpha^s = T$ :  $T_\beta^s = (1 - \varepsilon)T$ ;  $T_\alpha^D = \lambda T$ ;  $T_\beta^D = (1 - \varepsilon)\lambda T$ , we find the following form for  $\varepsilon$ ,

$$\varepsilon \propto 1 - \frac{F(E_0, E_1, E_2, E_3, E_{Fermi}^s, E_{Fermi}^d)}{\ln(\phi_T^s)T^2(1 + \lambda^2)}, \quad (12)$$

where  $F(E_0, E_1, E_2, E_3, E_{Fermi}^s, E_{Fermi}^d)$  is an algebraic function of all the energy parameters. The important feature to point out in Eq. 12 is the overall similarity with Eq. 8. The fact that a similar relationship between the coupling and anisotropy parameters of the system has been found from two very different approaches is remarkable: the creation of the relationship out of empirical analysis of the GME for the open system, and the analytical derivation from a bound state analysis of the eigenvalue equation.

The formation of the bound state can be linked to an interference effect between transmission resonances due to the presence of several transport channels in the system — a feature eluded to in Fig. 4. Resonances of this type have been observed in diverse systems such as in quantum billiards,<sup>24</sup> laser induced continuum structures in atoms,<sup>25</sup> and quantum dots.<sup>26</sup> In these works, it has been revealed that the formation of bound states in the continuum is directly related to the shape of the system and anisotropy of the coupling parameters. This point is specifically reflected in our findings as we only observe the FSC resonance under coupling anisotropies. These coupling anisotropies may play the role of a path difference between the channels, where specific path differences may quench transport through the system in an effect akin to negative differential conductance.<sup>27</sup> In such a case the FSC is enhanced — forming a resonance — since the dominant decoherence pathways are also effectively quenched. This may also help explain the presence of the single dominant resonance in the range of the orbital anisotropy in our model, since only a specific energy and coupling configuration will lead to transport quenching.

## VII. CONCLUSIONS

In conclusion, we have shown that the FSC of a fermionic system can be decoupled from the evolution of the population probabilities and the HSC of the system, even under the presence of boson-mediated relaxation and single-particle exchange with a bath. We demonstrated a resonant regime in this FSC where the decoherence times extend far beyond that of the HSC, and we have been able to relate these results to an analytically derived relationship in the coupling parameters of the system arising from the formation of a bound state between the system and reservoirs. We anticipate the primary difficulty in the experimental confirmation of our theory to be the establishment of the FSC in the first instance. What we have shown here is that such a FSC can exhibit a remarkable, robust, and long-lived resonance even in the presence of ordinarily very destructive perturbations such as particles tunnelling into and out of the system. A plausible configuration to obtain this FSC resonance effect is one where the particle reservoirs are macroscopic systems in thermodynamic equilibrium, as envisioned in the present work, and whose description is properly and most conveniently characterised by a particle density (not particle number) in a grand canonical ensemble. Subsequent experimental and further theoretical efforts extending this work may shed light on the fundamental problem of decoherence, and on quantum information processing in a semiconductor environment.

## ACKNOWLEDGMENTS

This work is supported by NSERC of Canada, and by Lockheed Martin Corporation.

---

\* <http://quantum.phys.dal.ca>

<sup>1</sup> P. Bertet, S. Osnaghi, P. Milman, A. Auffeves, P. Maioli, M. Brune, J. M. Raimond, and S. Haroche, *Phys. Rev. Lett.* **88**, 143601 (2002).

<sup>2</sup> M. Hofheinz, E. M. Weig, M. Ansmann, R. C. Bialczak, E. Lucero, M. Neeley, A. D. O'connell, H. Wang, J. M. Martinis, and A. N. Cleland, *Nature* **454**, 310 (2008).

<sup>3</sup> E. Bimbard, N. Jain, A. MacRae, and A. Lvovsky, *Nature Photon.* **4** (2010).

<sup>4</sup> S. Datta, *Fock space formulation for nanoscale transport* (2006), arXiv:cond-mat/0603034.

- <sup>5</sup> U. Harbola, M. Esposito, and S. Mukamel, Phys. Rev. B **74**, 235309 (2006).
- <sup>6</sup> V. Moldoveanu, A. Manolescu, and V. Gudmundsson, New J. Phys. **11**, 073019 (2009).
- <sup>7</sup> The FSC persists beyond the limit of our numerical calculations.
- <sup>8</sup> V. Moldoveanu, A. Manolescu, and V. Gudmundsson, Phys. Rev. B **82**, 085311 (2010).
- <sup>9</sup> We do not include Coulomb interactions among the confined particles. One reason for this is that a fully non-Markovian treatment of the dynamics of a model with explicit Coulomb interactions introduces an extraordinary level of complexity in the calculations, and we do not believe it qualitatively affects the Fock-space coherence we focus on in this work. For recent Markovian treatments of a model with explicit Coulomb interactions see Refs [28,29]. A second reason to neglect this particle-particle interaction is that that our results remain valid in configurations where the dot, in equilibrium, is occupied by zero or one fermions.
- <sup>10</sup> The tunnelling coefficient may be written with an additional index labelling the reservoir state. However, for the parameter regime in which we focus, the variation of the tunnelling coefficient with dot orbitals is much greater than that with the lead states.
- <sup>11</sup> E. Vaz and J. Kyriakidis, Phys. Rev. B **81**, 085315 (2010).
- <sup>12</sup> Eduardo Vaz and Jordan Kyriakidis, unpublished.
- <sup>13</sup> J. Kyriakidis, M. Pioro-Ladriere, M. Ciorga, A. S. Sachrajda, and P. Hawrylak, Phys. Rev. B **66**, 035320 (2002).
- <sup>14</sup> One additional element,  $\rho_{02}$ , describing states differing by two confined particles is additionally not depicted. Such elements form in still other isolated blocks. The overall block diagonal structure is maintained for *arbitrary* numbers of transport channels differing by arbitrary number of confined particles.
- <sup>15</sup> We numerically evaluate the Bromwich integral using an adaptive Fourier integration routine and tables of Chebyshev moments. See, for example, the QAWF algorithms in the GNU scientific library (<http://www.gnu.org/software/gsl>).
- <sup>16</sup> We impose the equality  $T_{\beta}^s/T_{\alpha}^s = T_{\beta}^d/T_{\alpha}^d$  solely for reasons of simplicity.
- <sup>17</sup> M. Ciorga, A. Wensauer, M. Pioro-Ladriere, M. Korkusinski, J. Kyriakidis, A. S. Sachrajda, and P. Hawrylak, Phys. Rev. Lett. **88**, 256804 (2002).
- <sup>18</sup> D. Auston, and M. Nuss, IEEE J. Quantum Electron. **24** 184 (2010).
- <sup>19</sup> Ulbricht R, Hendry E, Shan J, Heinz T F and Bonn M, Rev. Mod. Phys. **83** 543–586 (2011).

- <sup>20</sup> A. Dienst, M. C. Hoffmann, D. Fausti, J. C. Petersen, S. Pyon, T. Takayama, H. Takagi, and A. Cavalleri, *Nature Photon.* **5**, 8 485–488 (2010).
- <sup>21</sup> M. Miyamoto, *Phys. Rev. A* **72**, 063405 (2005).
- <sup>22</sup> E. N. Bulgakov, I. Rotter, and A. F. Sadreev, *Phys. Rev. A* **75**, 067401 (2007).
- <sup>23</sup> Q. J. Tong, J. H. An, H. G. Luo, and C. H. Oh, *Phys. Rev. A* **81**, 052330 (2010).
- <sup>24</sup> A. F. Sadreev, E. N. Bulgakov, and I. Rotter, *Phys. Rev. B* **73**, 235342 (2006).
- <sup>25</sup> A. I. Magunov, I. Rotter, and S. I. Strakhova, *J. Phys. B* **32**, 1669 (1999).
- <sup>26</sup> I. Rotter, and A. F. Sadreev, *Phys. Rev. E* **71**, 046204 (2005).
- <sup>27</sup> E. Vaz, and J. Kyriakidis, *J. Chem. Phys.* **129**, 024703 (2008).
- <sup>28</sup> M. Esposito, and M. Galperin, *Phys. Rev. B* **79**, 205303 (2009).
- <sup>29</sup> G. Bulnes Cuetara, M. Esposito, and P. Gaspard, *Phys. Rev. B* **84**, 165114 (2011).